Flowfield Measurements for a Highly Turbulent Flow in a Stator Vane Passage

R. W. Radomsky and K. A. Thole
Mechanical Engineering Department
University of Wisconsin
Madison, Wisconsin 53706

Abstract

Turbine vanes experience high convective surface heat transfer as a consequence of the turbulent flow exiting the combustor. Before improvements to vane heat transfer predictions through boundary layer calculations can be made, we need to understand how the turbulent flow in the inviscid region of the passage reacts as it passes between two adjacent turbine vanes. In this study, a scaled-up turbine vane geometry was used in a low-speed wind tunnel simulation. The test section included a central airfoil with two adjacent vanes. To generate the 20% turbulence levels at the entrance to the cascade, which simulates levels exiting the combustor, an active grid was used. Three-component laser Doppler velocimeter measurements of the mean and fluctuating quantities were measured in a plane at the vane mid-span. Coincident velocity measurements were made to quantify Reynolds shear stress and correlation coefficients. The energy spectra and length scales were also measured to give a complete set of inlet boundary conditions that can be used for numerical simulations. The results show that the turbulent kinetic energy throughout the inviscid region remained relatively high. The surface heat transfer measurements indicated high augmentation near the leading edge as well as the pressure side of the vane as a result of the elevated turbulence levels.

Introduction

High heat transfer augmentations on a turbine blade due to the turbulence levels exiting the combustor continues to be a topic of concern for the gas turbine industry. With this concern comes the need to develop a fundamental understanding of how the highly turbulent flow convects through the turbine vane passage. The turbulence characteristics in the inviscid flow region of the turbine vane passage are typically needed as a boundary condition for boundary layer calculations. Also, when performing a full Navier-Stokes CFD simulation, one of the first benchmarks needed for the various turbulence models is a comparison of the turbulence predictions in the passage.

This paper presents mean and turbulent flowfield measurements in the inviscid region of the turbine airfoil for both a low (baseline) and a highly turbulent flowfield. Several studies presented in the past have measured two of the three velocity components with rms levels in a scarce number of locations in a turbine vane passage. In this study, all three fluctuating velocities were measured to quantify the turbulent kinetic energy variation in the turbine vane passage. Coincident streamwise and cross-pitch velocities were measured to quantify Reynolds shear stress. Energy spectra of the fluctuating velocities were computed to give length scales and estimates of the dissipation at the entrance to the turbine vane. These measurements provide an understanding of the variation of the turbulence throughout the passage as well as a complete set of inlet boundary conditions necessary for a numerical simulation.

Past Studies

There have been a few studies documenting turbulence levels exiting the combustor. Kuotmos and McGuirk (1989) measured mean and fluctuating velocity profiles in a can-type combustion chamber and reported local axial turbulence levels up to 30% at the exit of the combustor. Moss (1992) also measured turbulence levels exiting a variety of gas turbine combustors and reported turbulence levels of 9% with a typical length scale being between 5 to 7 mm giving a length scale to pitch ratio of $0.1 < L_x/P < 0.14$ for a typical first stage stator vane. Ames (1995) studied turbulence levels exiting a scaled-up, two dimensional representation of an annular combustor and reported turbulence levels as high as 13% with a length scale to pitch ratio of $L_x/P = 0.13$.

The characteristics of the turbulent field convecting through the passage have not been completely documented at this time. Bailey (1980), Priddy and Bayley (1988), Ames (1994), Bangert, et al. (1997), and Radomsky and Thole (1998) all reported measurements of some turbulence components inside the turbine vane passage. All of these studies reported that there is a decrease in the streamwise fluctuations in the inviscid region as the flow accelerates along the suction side of the vane. Along the pressure side of the vane, Priddy and Bayley (1988) reported streamwise fluctuations that remained nominally constant. Ames (1994) reported an increase in the cross-stream fluctuations (normal to the blade surface) as the flow progressed through the passage, while Radomsky and Thole (1998) reported similar increases in both the cross-stream and spanwise fluctuations.

In general, there is still not enough information known regarding the turbulent flowfield characteristics surrounding a turbine airfoil. To date, there have been some measurements of the streamwise fluctuations and a scarce number of measurements of the cross-pitch velocity fluctuations. Not enough measurements have been made to deduce the turbulent kinetic energy field or the shear stress surrounding a vane. There is a need to have well-documented turbulent flowfield measurements to both gain a better physical understanding as well as for CFD benchmarking purposes.

Experimental Facility and Instrumentation

A stator vane, scaled up by a factor of nine, was placed in a large-scale wind tunnel for this study. The stator vane geometry was a two-dimensional slice of an engine profile taken at the vane midspan. The construction and the development of the scaled-up stator turbine vane and the test section have been previously documented by Radomsky and Thole (1998) and Kang, et al. (1998). The wind tunnel used in this study is recirculating with a corner test section, shown in Figure 1. This test section contains a central turbine vane with two adjacent vanes. The outside adjacent vane was constructed by attaching a leading edge to a plexiglass sidewall allowing for optical access. The placement of the sidewall exactly matches that surface of an adjacent vane. At the point where the adjacent vane geometry stops, the flexible wall was positioned such that the central vane matched a two-dimensional, inviscid pressure distribution computationally predicted for periodic vanes at low-speed conditions. The inlet Reynolds number, based upon approach velocity and chord length, was matched to that of engine conditions. Pressure measurements on the central vane were made to ensure that the sidewall and flow stagnation point were positioned correctly. The upstream sidewall boundary layers were removed by adjustable bleeds while tailboards on the outer vanes ensured that periodic flow occurred in both passages around the central airfoil. A description of the turbine vane itself is given by Table 1.

A fixed cartesian coordinate system was maintained for these measurements based on a location measured from the flow stagnation point, as shown in Figure 1. Flowfield measurements, which included all three velocity components and rms velocities, were performed with a two-component laser Doppler velocimeter (LDV) with digital burst correlator processors. The LDV was positioned both on the top of the test section to measure the streamwise (U) and cross-passage (V) velocity components and on the side of the test section to measure spanwise (W) velocities. A 350 mm focusing lens without a beam expander was used to make measurements of the streamwise and pitchwise components through the top endwall. The spanwise component was measured from the side using the 750 mm focusing lens with a beam expander. The probe volume length and diameter for the 350 mm lens were 1.3 mm and 90 microns whereas the probe volume length and diameter for the 750 mm lens with the beam expander were 0.85 mm and 46 microns. The flow was seeded with 1 micron diameter aluminum dioxide particles. The measured velocities were corrected for bias errors using the residence time weighting correction scheme.

Table 1. Geometrical and Flow Conditions for the Stator Vane Geometry.

Scaling factor	9
Scaled-up chord length (C)	59.4 cm
Pitch / chord (P/C)	0.77
Span / chord (S/C)	0.93
Re_{in}	2.30×10^5
Inlet and exit angles	0° and 78°

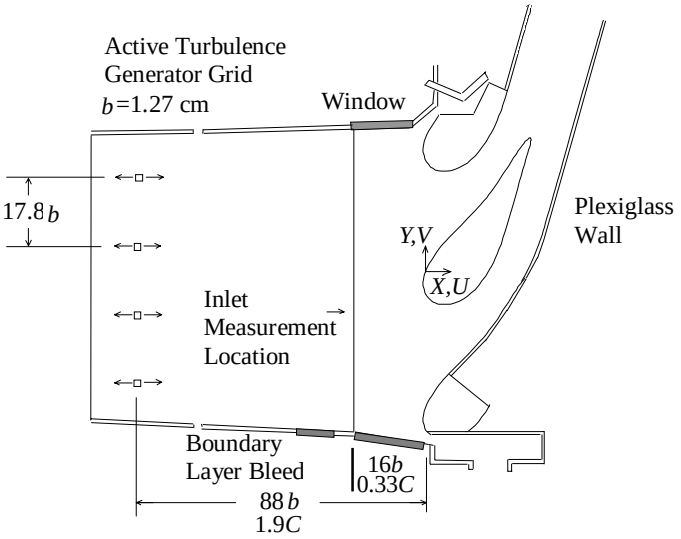

Figure 1. Schematic of stator vane test section.

Nomenclature

b	turbulence generator bar width
C	True chord length
e	Emissivity
$E_1(k_1)$	Spectra for streamwise fluctuations
f	Frequency
h	Convective heat transfer coefficient, $h = q\dot{q}_{conv}/(T_s - T_\infty)$
k	Turbulent kinetic energy, $k = 0.5(u_{rms}^2 + v_{rms}^2 + w_{rms}^2)$
k_1	Wavenumber, $k_1 = 2\pi f/u$
L_e	Dissipation length scale, $L_e = 1.5u_{rms}^3/\varepsilon$
P	Turbine vane pitch
$q\dot{q}_{conv}$	Convective heat flux, $q\dot{q}_{conv} = q\dot{q}_{input} - q\dot{q}_{rad} - q\dot{q}_{cond}$
$q\dot{q}_{cond}$	Conductive heat flux from finite element analysis
$q\dot{q}_{input}$	Total heat flux from foils
$q\dot{q}_{rad}$	Radiative heat flux, $q\dot{q}_{rad} = \varepsilon\sigma(T_s^4 - T_\infty^4)$
R	Radius of curvature
R_{uv}	Turbulent correlation coefficent, $R_{uv} = \overline{u'v'}/(u_{rms}v_{rms})$
Re_{in}	Reynolds number based on chord length and inlet velocity
Re_λ	Reynolds number based on Taylor microscale and u_{rms}
s	Distance measured along vane surface from stagnation
S	Full span
St	Stanton number, $h/\rho C_p U_\infty$
T_s	Surface temperature
T_∞	Freestream temperature
Tu	Turbulence Level
U_∞	Upstream incident velocity
$\overline{u'v'}$	Reynolds shear stress
u,v,w	Local mean velocities along a streamline
U,u_{rms}	Local mean and rms velocities in the X-direction
V,v_{rms}	Local mean and rms velocities in the Y-direction
W,w_{rms}	Local mean and rms velocities in the Z-direction
X,Y,Z	Fixed Cartesian coordinate system measured from the flow stagnation, see Figure 1.

Greek

ε	Turbulent dissipation obtained from equation (1)
Λ_x	Streamwise integral turbulent length scale
λ	Taylor microscale
ν	Kinematic viscosity
σ	Stefan-Boltzman constant

Autocorrelation length scales were measured with a single sensor hot-wire having a length of 1.5 mm and diameter of 4 microns. The hot-wire sensor had a frequency response of 200 kHz at 36 m/s, but the analog output was filtered at 10 kHz. The integral length scales were calculated using eight samples with each sample having 80,000 points at a sample frequency of 20 kHz. These single sensor hot-wire measurements were taken at a position where the flow was only in one direction based on the assumption of a Guassian distribution of the turbulence. As will be shown later, good agreement occurred for both the mean and rms levels between the hot-wire measurements and LDV measurements.

As previously described by Radomsky and Thole (1998), the central vane as well as the outer leading edges were constructed by stacking rigid polystyrene pieces 5 cm thick that were cut into the shape of the vane using a template and a heated wire. On the outside of the central vane surface, five 50 mm thick type 304 stainless steel foils were attached to the polystyrene. The metal foils provided a constant heat flux boundary condition. Beneath the stainless steel foil and embedded in the styrofoam 58 type E thermocouples were placed. The spanwise position for the thermocouples was at 40% of the span measured from the bottom endwall.

The convective heat flux was calculated using the total power supplied to the metal foils minus radiation losses and conduction losses and gains. The radiation correction used a vane surface emissivity of $e = 0.22$ (value for typical clean stainless steel given by Incoprera and DeWitt, 1996) and the measured side wall temperatures which agreed with the freestream temperature. The radiation losses ranged between 3 - 8% of the input power for the baseline, low turbulence cases. A two-dimensional finite element grid was constructed to account for the conduction losses and gains. The worst case was for the baseline case close to the trailing edge resulting in a 2% correction.

The development of the turbulence generator used for the high freestream turbulence experiments was described in detail by Bangert, et al. (1997). This active grid consists of vertical hollow square bars with jets injecting into the mainstream in both the upstream and downstream directions. The bars are 1.27 cm square with the jet holes having a diameter of 1.5 mm and vertically spaced 3.05 cm apart. These hollow bars were installed 88 bar widths upstream of the stator vane stagnation position or, in terms of vane coordinates, at 1.9 chords in front of the stagnation position. A compressed air supply fed a plenum that supplied each of the bars.

Uncertainty Estimates

Each of the mean and rms velocities presented in this paper were averaged over 12,000 points which took nominally 30 seconds to acquire using the LDV. When performing coincidence measurements for the Reynolds shear stress, a total of 25,000 points were taken at each location. The precision uncertainties for these measurements were estimated using a 95% confidence interval. The precision uncertainty for the mean velocities was 0.7% for the low turbulence measurements and 0.8% for the high turbulence level while the bias uncertainty for both was estimated to be 1%. The precision uncertainty for the rms of the velocity fluctuations was 2.0% for the high turbulence levels, while the uncertainties in the measured Reynolds stress and turbulent correlation coefficient were estimated to be 12%. For the hot-wire measurements, the precision uncertainty for the mean and rms velocities were 2.6% and 2.5% respectively, while the uncertainty in the integral length scale was estimated to be 12.4%.

The total uncertainty in Stanton numbers, using the sequential perturbation method discussed by Moffat (1988) was 4% at the leading edge and 5% at the trailing edge on the suction side of the vane. The higher uncertainty at the trailing edge of the suction side is a result of the lower difference between the surface and mainstream temperatures which dominated the uncertainty in the Stanton number.

Inlet Flow Conditions

To insure good flow conditions around the turbine vane, a number of velocity profiles were checked upstream and at the stagnation location. Mean velocity profiles were measured for low and high turbulent flowfields at the inlet using both an LDV and a hot-wire anemometer. In addition, flowfield measurements were compared between the inner and outer passages to insure good periodicity in the two passages surrounding the central vane. The flowfield measurements were compared with CFD predictions made using RAMPANT as described in FLUENT/UNS (1996). These two-dimensional, inviscid, CFD predictions were made for the low freestream turbulence case using a single passage with periodic boundary conditions. The inlet velocities to the turbine vane for both the low and high turbulence cases were matched.

Figure 2a compares measured and predicted profiles across the entire pitch of the two passages in terms of the streamwise and cross-stream velocities normalized by the upstream incident velocity, U_∞. The measurement location was one-third of a chord upstream of the vane stagnation. Both the low and high freestream turbulence cases are presented in Figure 2a. The velocity measurements for both the low and high turbulent cases agree very well with the predicted velocities except near the edge of the test section where there is a sidewall boundary layer. Note that this is upstream of the sidewall suction slot, which is intended to remove the sidewall boundary layer. These measurements are a good indication that the active grid jets have not affected the mean flowfield. Across the vertical span of the turbine vane, the mean velocity uniformity was such that the maximum deviation normalized by the average velocity was 1.6% and 3.5% for the low and high turbulence cases. In addition to the LDV data, Figure 2a shows good agreement with the hot-wire measurements of the streamwise velocity component for the highly turbulent case. At this location, the vane is already detected by the flow showing a deceleration in the streamwise velocity component at the center of the passage. As the streamlines turn around the vane, slightly positive cross-span (V/U_∞) velocities occur near the stagnation for $Y/P > 0$ and slightly negative cross-span velocities occur near the stagnation for $Y/P < 0$.

Figure 2b shows the normalized rms levels of the streamwise (u_{rms}/U_∞), cross-stream (v_{rms}/U_∞), and the spanwise (w_{rms}/U_∞) velocity fluctuations as well as the normalized integral (Λ_x / P) and dissipation (L_ε / P) length scales for the highly turbulent case. At the inlet location, all three rms levels are close to the same value with only slightly lower spanwise fluctuations, w_{rms}/U_∞. The average spanwise fluctuations are 91% of the average streamwise fluctuations and 93% of the cross-stream fluctuations. For the high turbulent case, the maximum deviation of the rms velocities across the vertical span of the turbine vane was 2.8%. The

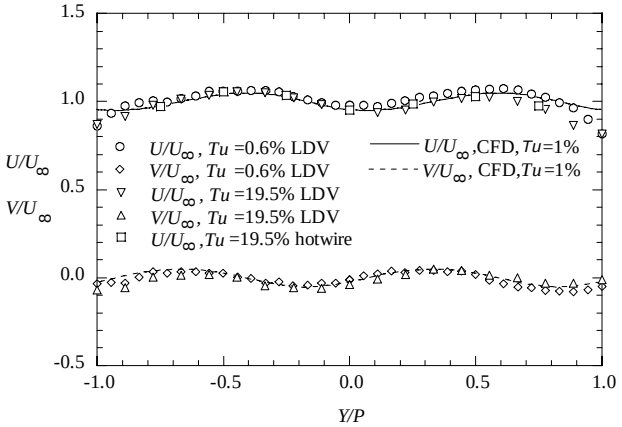

Figure 2a. Inlet mean velocity profiles measured at one-third chord upstream of the vane stagnation.

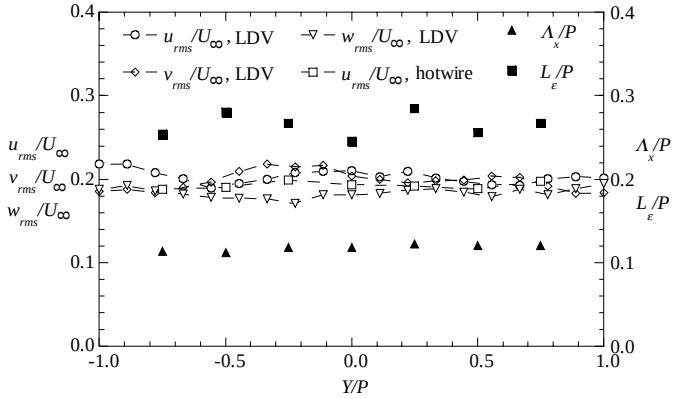

Figure 2b. Inlet turbulence levels and length scale measured at one-third chord upstream of the vane stagnation.

average turbulence level at this location is 19.5%. The hot-wire measurements of the streamwise fluctuations in Figure 2b show good agreement with the LDV measurements.

The integral length scale, also shown in Figure 2b, is nominally 12% of the vane pitch and is relatively uniform across the pitch. The dissipation, used in the dissipation length scale, was determined from a curve fit to the following formula in the inertial subrange of the energy spectra for the streamwise fluctuations (Hinze, 1975 and Ames, 1994):

$$E_1(k_1) = 1.62\ (18/55)\varepsilon^{2/3}\ k_1^{-5/3} \qquad (1)$$

The dissipation length scale is nominally two times larger than the integral length scale. Figure 2b shows that the level and scale of the turbulence are representative of combustor generated turbulence as measured by Moss (1992) and Ames (1995).

Figure 3a shows LDV mean velocity measurements across the passages at the vane geometric stagnation for both the low and high turbulence cases as compared with a CFD prediction for the low turbulence case. Note that both the inside and outside passages around the central turbine vane are shown. There is good agreement between the measured and predicted mean velocity components as well as an indication that the flow periodicity between the two passages is quite good. The rms velocities for the highly turbulent flowfield also showed good periodicity for the two passages, as will be shown later.

Streamwise velocity measurements leading up to the flow stagnation and mid-span passage locations of the vane are compared with that predicted in Figure 3b. Note that good agreement between the predicted and measured velocities using both the LDV and hot-wire occur. Figure 4 shows how the streamwise rms levels of the velocity fluctuations as well at the turbulent kinetic energy, normalized by the upstream velocity, vary proceeding up to the leading edge. For each of the velocity fluctuations, an increase starts to occur at X/C = -0.05 moving towards the vane. Very close to the vane, the streamwise fluctuations, u_{rms}/U_∞, again decrease. Note that the hot-wire measurements of the streamwise fluctuations are only presented up to X/C = -0.1. Beyond that location the streamlines turn significantly and the velocities are quite low with high turbulence levels making the hot-wire measurements invalid. The turbulent kinetic energy, also shown in Figure 4, increases to a level that is 1.3 times higher than at the inlet. The rapid increase starts to occur at approximately one integral length scale upstream of the vane stagnation ($X/C \sim$ -0.1).

The energy spectra of the streamwise fluctuations at the inlet are shown in Figure 5 as compared with the von Karman spectra and the unified relation given by Mayle et al. (1997). Also shown in Figure 5 is

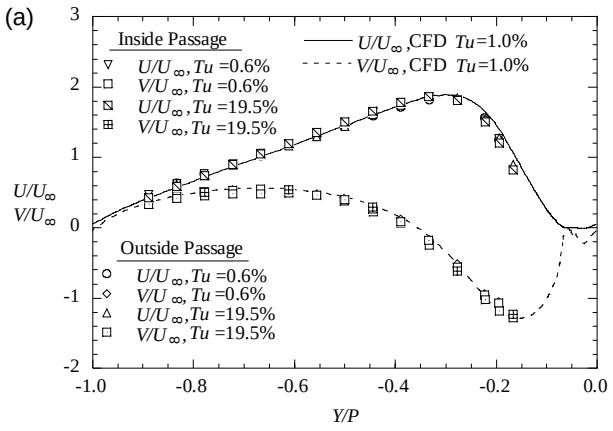

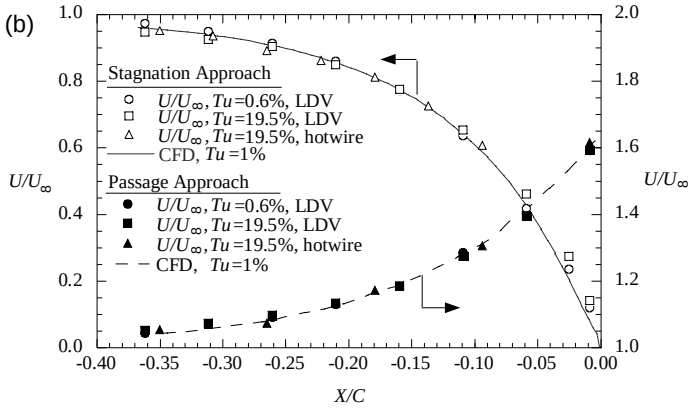

Figure 3. (a) Velocity components measured at the geometrical stagnation and (b) velocity approaching the vane stagnation and passage.

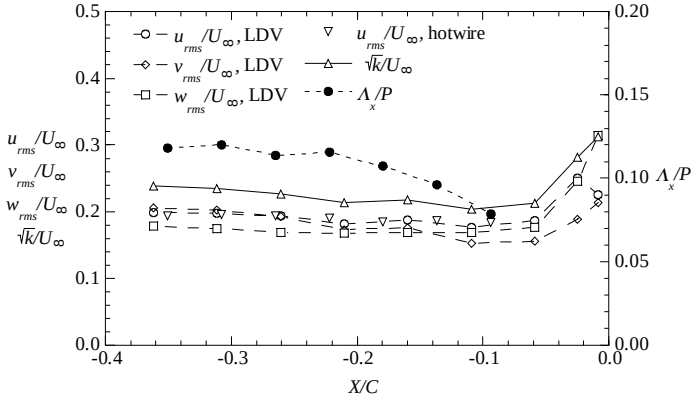

Figure 4. RMS velocity components, turbulent kinetic energy and integral length scale approaching the vane stagnation point.

the spectra taken at the closest position to the stagnation location. The turbulent Reynolds numbers, Re_l, for these two locations are quite similar. The Taylor microscale was estimated from the following relation:

$$\lambda = \left[\frac{15 \nu u_{rms}^2}{\varepsilon} \right]^{1/2} \quad (2)$$

In the low wave number region there is good agreement between the measured energy spectra and those given by the von Karman and Mayle et al. (1997) relations. As the wave number increases, the drop-off of the inertial subrange is well predicted by the relation given by Mayle, et al. for the inlet condition (*X/C* = -0.35). Although the turbulent Reynolds numbers are very similar, closer to the stagnation location (*X/C* = -0.09) the drop-off in the inertial subrange is not predicted by the relation given by Mayle, et al. (1997) but is much more rapid.

Mean Velocity Flow Field Results

Figures 6a and 6b show vectors and normalized total velocity contours for the low freestream turbulence case measured throughout the passage. Note that all of these flowfield measurements were made in a plane at the midspan between the midpitches of the central vane passages. For presentation purposes in this paper the data was simply numerically shifted to give one full pitch from stagnation to stagnation. Because the data was shifted, the smoothness of the contours are an indication of the good flow periodicity in both passages of the central vane.

As expected with this vane geometry, there is a high acceleration that occurs around the suction side of the vane. The flow stagnation can be clearly seen from both the contours and the velocity vectors. The contour levels indicate that the flow has been accelerated to five times the incident velocity.

Figure 7 gives the normalized total velocity contours for the highly turbulent flow. The largest difference between Figures 6b and 7 is along the suction surface where a larger region of high speed fluid occurs for the highly turbulent flowfield. This larger high speed region is a result of an acceleration of the inviscid flow due to the transition of a turbulent boundary layer occurring further upstream along the vane. Earlier transition caused a thicker turbulent boundary layer along the suction side of the vane for the highly turbulent case. The difference between the cases can also be seen in Figure 8 where the local freestream velocity distribution is given for the measured conditions and the inviscid CFD prediction. The effect of the larger boundary layer thickness can be seen at values greater than *s/C*=0.5.

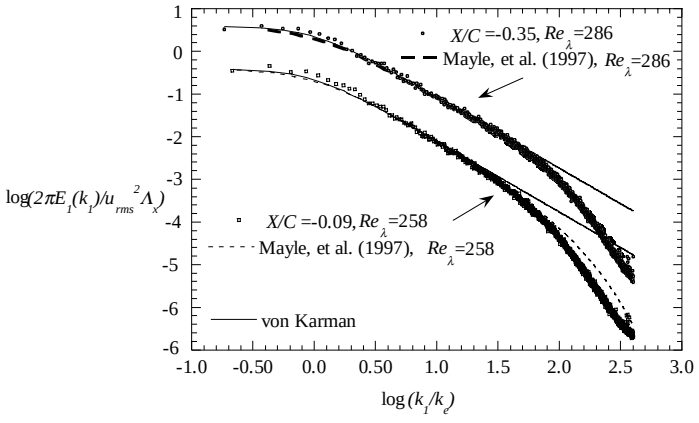

Figure 5. One-dimensional energy spectra approaching the vane stagnation point.

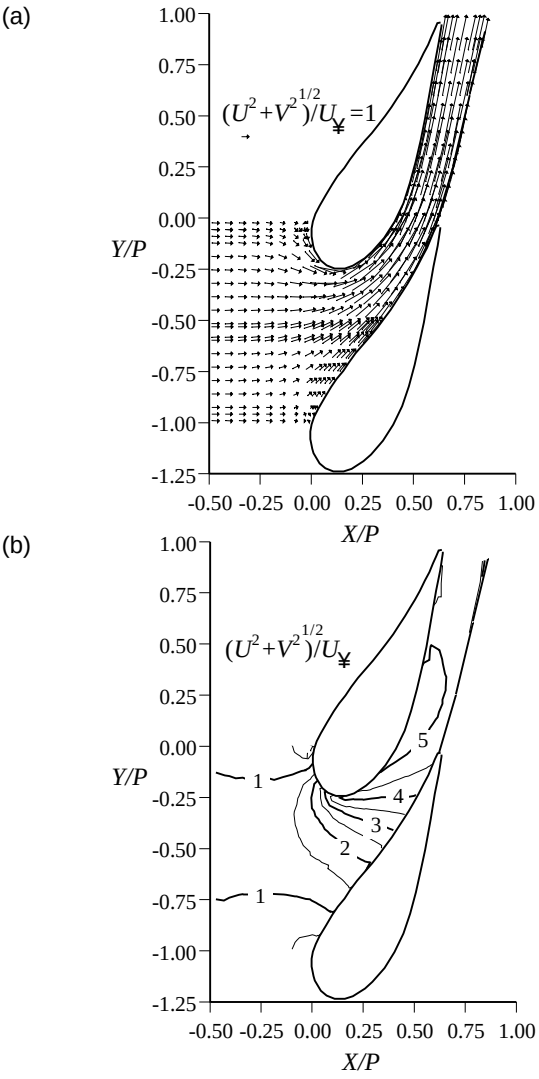

Figure 6. (a) Total velocity vectors and (b) total velocity contours at *Tu*=0.6%

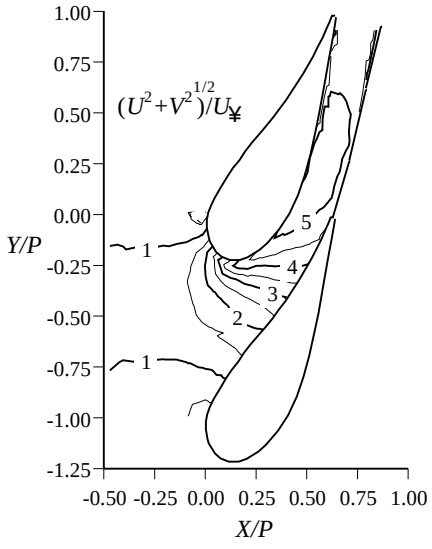

Figure 7. Total velocity contours at *Tu*=19.5%

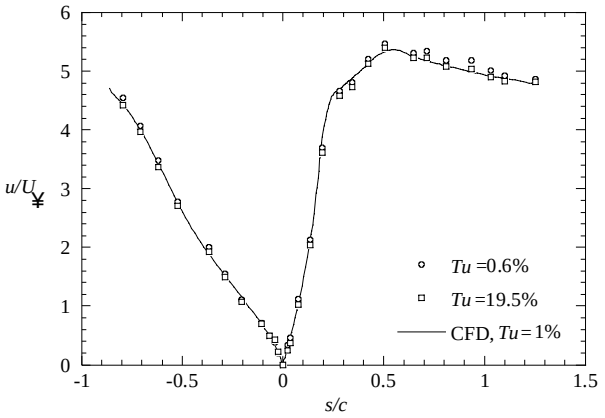

Figure 8. Vane velocity distribution at *Tu*=0.6% and *Tu*=19.5%

Turbulent Flow Field Results

Contours of the rms levels of the fluctuations for each of the velocity components were measured for the inviscid region. Figures 9a - 9c show contour levels of the normalized rms levels for the 19.5% inlet turbulence case. Contour levels are given in increments of 0.04.

For the streamwise fluctuations, shown in Figure 9a, the inlet levels are nominally $u_{rms}/U_{¥} = 0.2$. Between the inlet and stagnation region the rms levels are between $u_{rms}/U_{¥} = 0.16$ and 0.20. Near the leading edge, an increase in the streamwise fluctuations occurs with the peak occurring just upstream of the geometric stagnation location towards the suction surface of the vane relative to the flow stagnation location. The peak level rises to a value of $u_{rms}/U_{¥} = 0.24$. Very near the geometric stagnation point, the streamwise fluctuations decrease as a result of being attenuated by the presence of the vane. As the flow progresses along the pressure surface the $u_{rms}/U_{¥} = 0.20$ contour level moves away from the pressure surface giving a lower value of $u_{rms}/U_{¥} = 0.16$. At the mid-pitch of the passage the lowest streamwise rms levels occur at $u_{rms}/U_{¥} = 0.12$. This region is where the flow begins to turn and has the highest acceleration in the streamwise velocity component resulting in a negative production of the streamwise velocity fluctuations.

Progressing through the passage, the streamwise fluctuations again start to increase up to a peak of $u_{rms}/U_{¥} = 0.28$. Beyond that peak location, the rms levels stay relatively constant. Note that near the suction surface, the streamwise rms levels are lower than at the mid-portion of the passage. Keeping in mind that an orthogonal coordinate system was maintained for these measurements, these velocity fluctuations are almost normal to the vane surface. The lower values near the surface can be explained by the fact that the vane surface is attenuating the fluctuations.

The cross-stream rms contours are shown in Figure 9b. Again, there is good uniformity at the entrance to the test section with a level of $v_{rms}/U_{¥} = 0.20$. A high contour of $v_{rms}/U_{¥} = 0.24$ occurs near the shoulder of the stator vane in the high acceleration region. This is also the location of the low contours of $u_{rms}/U_{¥}$. Also, a low contour of $v_{rms}/U_{¥} = 0.12$ occurs in the middle of the passage which starts at the location where the high contour of $u_{rms}/U_{¥}$ occurred. Near the suction side of the vane surface, very high $v_{rms}/U_{¥}$ values occur. Unlike the $u_{rms}/U_{¥}$ fluctuations, which were being attenuated at the vane surface, the cross-stream fluctuations are quite high at the suction surface. These high values occur near the end of the turbine vane suction surface since this direction is more parallel with the turbine vane surface.

The spanwise rms contours, shown in Figure 9c, indicate variations only occurring in the near-wall regions. At the inlet the levels are $w_{rms}/U_{¥} = 0.16$ with values becoming slightly higher at $w_{rms}/U_{¥} = 0.20$ once inside the passage.

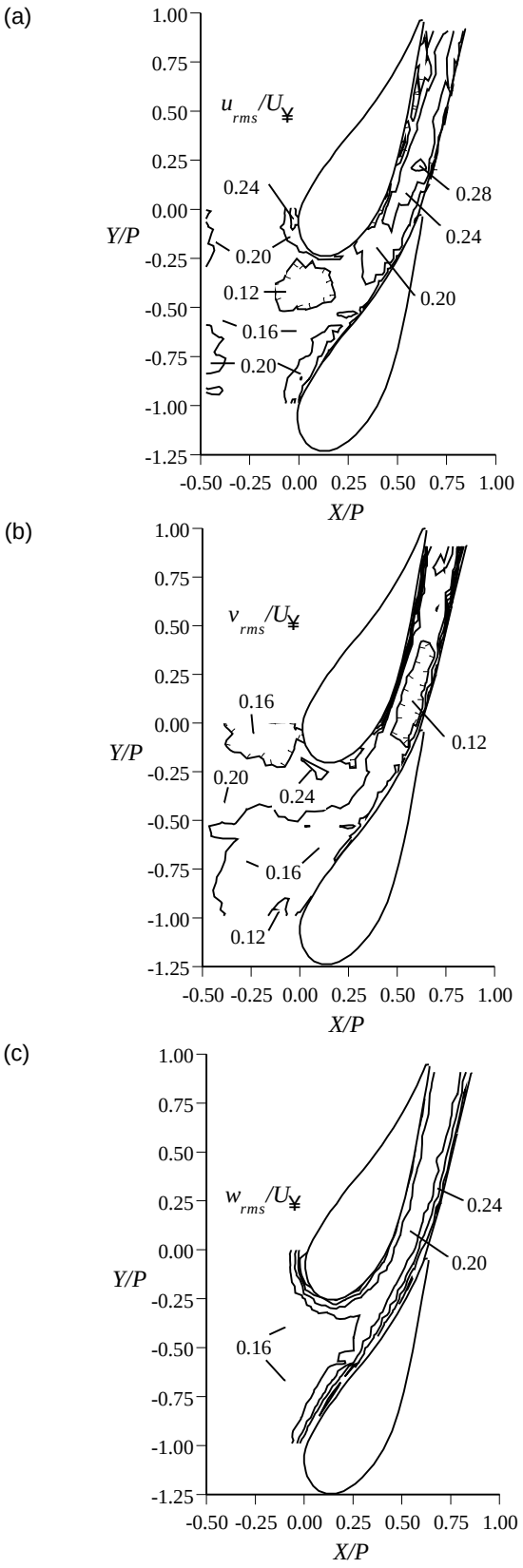

Figure 9. (a) Contours of (a) $u_{rms}/U_{¥}$, (b) $v_{rms}/U_{¥}$ and (c) $w_{rms}/U_{¥}$ at *Tu*=19.5%

The turbulent kinetic energy level contours, which combine all three fluctuations, are shown in Figure 10. Note that the increment between levels is 0.02. These contours are presented in terms of $\sqrt{k}/U_\infty$ and can be converted to a turbulence intensity through multiplying by a constant factor, i.e. $\sqrt{2/3}\sqrt{k}/U_\infty$. The turbulent kinetic energy is quite uniform at the inlet with values between $\sqrt{k}/U_\infty$ = 0.22 and 0.24. As the flow progresses towards the geometrical stagnation on the suction side of the vane the turbulent kinetic energy levels increase significantly reaching as high as $\sqrt{k}/U_\infty$ = 0.32. At the mid-pitch region just upstream of the passage, lower turbulent kinetic energy levels occur with values as low as $\sqrt{k}/U_\infty$ = 0.20. Once inside the vane passage the turbulent kinetic energy increases to a level of $\sqrt{k}/U_\infty$ = 0.26 and remains essentially constant throughout the middle of the passage. This result shows that there is not a decay in the turbulent kinetic energy through a turbine vane passage. Near the turbine vane walls high values of the turbulent kinetic energy were measured. It is clear that there is a very high region along the suction side of the vane beyond *s/C* = 0.4 which is approximately where transition to a turbulent boundary layer occurs.

Coincident LDV data were taken for the *U* and *V* velocity components to quantify Reynolds shear stress and correlation coefficients. Contours of the Reynolds shear stress normalized by the square of the inlet mean velocity ($\overline{u'v'}/U_\infty^2$) are shown in Figure 11a while the correlation coefficients (R_{uv}) are shown in Figure 11b. Unlike the other turbulent stress components (u_{rms}^2, v_{rms}^2, and w_{rms}^2), the shear stress contours indicate a much different behavior. Positive shear stresses occur along the shoulder of the suction surface starting at the flow stagnation location. A negative shear stress occurs beyond this location. In the center of the passage, the magnitude in shear stress increases up to $|\overline{u'v'}|$ = 0.03 after which a decrease occurs.

For the turbulent shear stress, $\overline{u'v'}$, it is helpful to consider the production mechanism under high freestream turbulence conditions. As pointed out by Gibson and Rodi (1981) and Bradshaw (1973), the production term for $\overline{u'v'}$ along a streamline can be written as,

$$P(\overline{u'v'}) = (2u_{rms}^2 - v_{rms}^2)\frac{u}{R} - v_{rms}^2\left[(1+\frac{y}{R})\frac{\partial u}{\partial y}\right] \qquad (3)$$

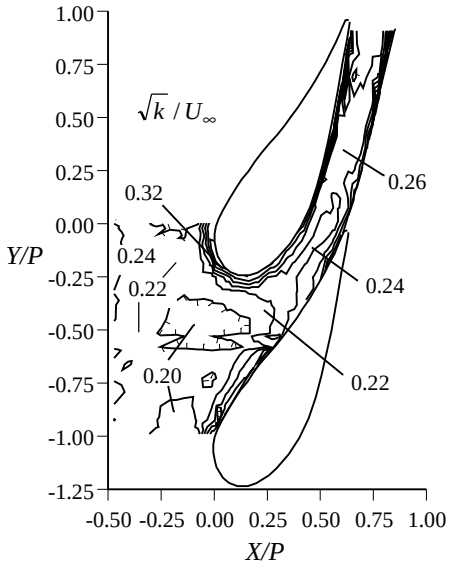

Figure 10. Contours of $\sqrt{k}/U_\infty$ at *Tu*=19.5%

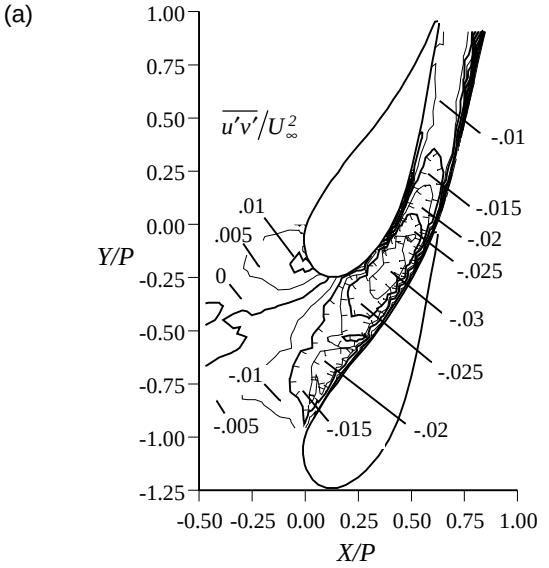

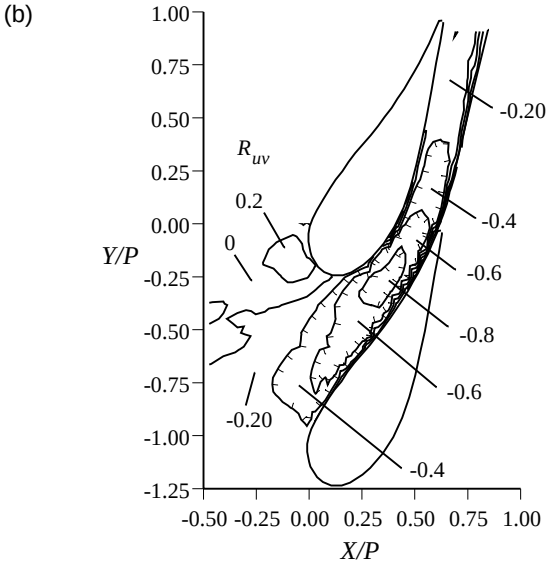

Figure 11. Contours of (a) $\overline{u'v'}/U_\infty^2$ and (b) R_{uv}.

In considering the inviscid region for the high turbulent case, the dominant term in this production equation is the first term whereby streamline curvature effects are included. For equation (3), *R* is the radius of curvature of the streamlines, positive for convex curvature and negative for concave curvature; and *u*, *v*, and *w* are the local mean velocity components along the streamline. In the case where the freestream turbulence level is low but yet the flow has streamline curvature, the production of $\overline{u'v'}$ shear stress is quite small. In the case where there is no streamline curvature but yet the flow has high freestream turbulence levels, the production of $\overline{u'v'}$ shear stress is also quite small. This latter case is indicated in the region upstream of the turbine vane and in the center of the vane passage where $\overline{u'v'}$ = 0 as shown in Figure 11a. As the flow approaches the turbine vane for the convex curved streamlines ($R > 0$) along the suction surface shoulder, a positive production occurs as $2u_{rms}^2 > v_{rms}^2$. Much further into the passage where concave curved streamlines occur

(R < 0) and $2u_{rms}^2 > v_{rms}^2$, the production of $\overline{u'v'}$ decreases and the $\overline{u'v'}$ values approach zero.

An understanding of the turbulent kinetic energy contours is better achieved by considering the production terms for a curved streamline along with the shear stress contours. Gibson and Rodi (1981) and Bradshaw (1973) give the production term for the turbulent kinetic energy along a curved streamline as:

$$P(k^2) = \underline{-\overline{u'v'}\left[(1+\frac{y}{R})\frac{\partial u}{\partial y} - \frac{u}{R} + \frac{\partial v}{\partial s}\right]} - u_{rms}^2(\frac{\partial u}{\partial s} + \frac{u}{R}) - v_{rms}^2(1+\frac{y}{R})\frac{\partial v}{\partial y} \quad (4)$$

Gibson and Rodi as well as Bradshaw point out that the dominating production term is the one which is underlined. For a turbulent boundary layer on flat plate the production reduces to $\overline{u'v'}\partial u/\partial y$, but where curvature exists there are additional terms such as $\overline{u'v'}(u/R)$. For the convex curvature case (suction side of the vane) where R > 0 and $\overline{u'v'}$ > 0, this results in a positive production for the turbulent kinetic energy. For the concave curved streamlines where R < 0 and $\overline{u'v'}$ < 0, this also results in a positive production.

Referring to Figure 10, the lowest turbulent kinetic energy levels occur at a location of the mid-pitch entrance to the turbine vane passage. This location corresponds to the low shear stress values and very little streamline curvature. The high levels of turbulent kinetic energy near the geometric stagnation point (along the suction surface shoulder), can be attributed to the high turning of the streamlines. Progressing through the passage, as the shear stress increases there is an increase in the turbulent kinetic energy due to the increased production.

Figure 11b shows correlation coefficient contours. At the inlet to the turbine vane the turbulence structures are uncorrelated giving a correlation coefficient of R_{uv} = 0. Except for the suction shoulder of the turbine vane, the correlation coefficients were primarily negative with a peak reaching as high as $|R_{uv}|$ = 0.75. A negative correlation coefficient implies one of two conditions. The first condition is when a particle with a high U-velocity moves in the negative Y direction (negative V) giving a negative R_{uv} since the instantaneous U will be lower than $\overline{U}$. The second condition is when a low U-velocity fluid moves in the positive Y direction (positive V) which is towards the suction surface. Because of the cross-pitch pressure gradient driving the flow from the pressure side towards the suction surface, the streamlines move toward the suction surface. Based on this argument, one would expect negative correlation coefficients to occur inside the turbine vane passage. The correlation coefficient rapidly decreases at the end of the passage. In the leading edge region, the positive correlation coefficients occur because the low streamwise speed fluid is turning in the negative Y direction.

Flow Field Relative to Vane Heat Transfer

It has been well-documented that high freestream turbulence can greatly augment the surface heat transfer. Figure 12 shows the measured heat transfer along the vane surface for low and high freestream turbulence conditions. For the low freestream turbulence conditions, the peak heat transfer occurs at s/C = 0.25 which is where the highest acceleration occurs along the shoulder of the suction side of the turbine vane. For the high freestream turbulence conditions, the Stanton numbers are relatively constant at elevated values starting at the stagnation location and extending to s/C = 0.2 followed by a slight bump at s/C = 0.25. The transition location has significantly moved upstream on the vane surface for the high freestream turbulence conditions relative to the baseline low freestream turbulence. On the pressure side of the vane (s/C < 0), the

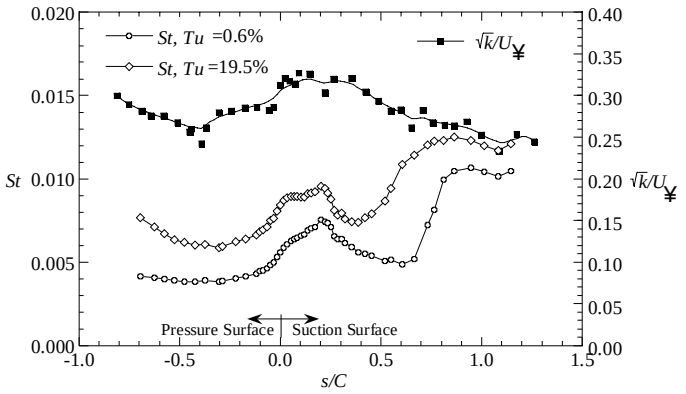

Figure 12. Stanton number distribution and turbulent kinetic energy outside the vane boundary layer.

Stanton numbers indicate a slight rise near the trailing edge of the vane surface indicating that transition may be starting.

Also shown in Figure 12 is the turbulent kinetic energy values along the turbine vane surface just outside of the boundary layer for the Tu = 19.5% case. The highest turbulent kinetic energy levels occur at the stagnation location extending along the suction side of the vane. The turbulence levels start to decrease at s/C = 0.4 and continue to decrease along the suction surface. After an initial decrease along the pressure surface, there is again an increase in the turbulent kinetic energy levels beyond s/C = -0.5. The highest augmentations in heat transfer occur along the pressure side of the vane where the increase in turbulent kinetic energy occurs.

Conclusions

This paper clearly showed that throughout the turbine vane passage, turbulence does not decay but rather it remains quite high throughout the passage. In order to conclude this, it was necessary to do a detailed flowfield mapping of all three velocities to quantify mean and rms levels. The turbulent kinetic energy contours showed increased values at the stagnation location and in the boundary layer after transition. The contours of streamwise and cross-pitch fluctuations showed variations throughout the passage which, along with the curvature of the streamlines, could be used to explain the production of the shear stress. The contours of spanwise fluctuations showed relatively constant values except near the turbine vane surface. The production mechanisms for the turbulent kinetic energy were also discussed whereby the streamline curvature played a significant role.

The turbulent correlation coefficients in the turbine vane passage indicate highly correlated turbulent structures exist. The sign of these coefficients are as expected with fluid moving from the pressure side of the vane to the suction side. The turbulent kinetic energy levels in the inviscid region just outside of the boundary layer show values that are very high with the peak levels occurring at the stagnation region and along the shoulder of the suction surface. Other than moving the transition location further upstream along the suction surface, the high freestream turbulence also greatly augmented the surface heat transfer along the pressure side of the vane.

Acknowledgments

The authors would like to thank the Department of Energy's Advanced Gas Turbine Systems Research Program for supporting this work. In particular, the authors would like to thank Dr. Dan Fant for serving as the contract monitor. The authors would also like to thank Pratt & Whitney, Florida for supplying the turbine vane geometry.

References

Ames, F.E., 1994, "Experimental Study of Vane Heat Transfer and Aerodynamics at Elevated Levels of Turbulence," NASA Contractor's Report 4633.

Ames, F. E., 1995, “The Influence of Large Scale High Intensity Turbulence on Vane Heat Transfer,” *ASME J of Turbomachinery*, vol. 119, pp. 23-30.

Bailey, D. A., 1980, “Study of Mean- and Turbulent- Velocity Fields in a Large-Scale Turbine-Vane Passage,” *ASME J of Engineering for Power*, vol. 102, pp. 88 - 95.

Bangert, B., Kohli, A., Sauer, J., and Thole, K. A., 1997, “High Freestream Turbulence Simulation in a Scaled-Up Turbine Vane Passage,” ASME Paper No. 97-GT-51.

Bradshaw, P., 1973, “Effects of Streamline Curvature on Turbulent Flow,” AGARD-AG-169.

FLUENT/UNS User’s Guide, 1996, Release 4.2, Fluent, Inc., Lebanon, N. H.

Gibson, M. M. and Rodi, W., 1981, “A Reynolds-Stress Closure Model of Turbulence Applied to the Calculationof a Highly Curved Mixing Layer,” *J of Fluid Mechanics*, vol. 103, pp. 161-182.

Hinze, J., 1975, Turbulence, 2nd Edition, (McGraw-Hill: New York).

Incropera, F. P. and DeWitt, D. P., 1996, Introduction to Heat Transfer, 3rd edition (John Wiley & Sons: New York).

Kang, M., Kohli, A., and Thole, K. A., 1998, “Heat Transfer and Flowfield Measurements in the Leading Edge Region of a Stator Vane Endwall,” ASME Paper No. 98-GT-173.

Kuotmos, P. and McGuirk, J. J., 1989, “Isothermal Flow in a Gas Turbine Combustor - A Benchmark Experimental Study,” *Experiments in Fluids*, vol. 7, pp. 344-354.

Mayle, R. E., Dullenkopf, K. and Schulz, A., 1997, “The Turbulence that Matters,” *ASME J of Turbomachinery*, vol. 120, pp. 402-409.

Moffat, R. J., 1988, “Describing Uncertainties in Experimental Results,” *Experimental and Fluid Science*, vol. 1, pp. 3 -17.

Moss, R. W., 1992, “The Effects of Turbulence Length Scale on Heat Transfer,” University of Oxford, Department of Engineering Science, Report No. OUEL 1924, Ph.D. Dissertation.

Priddy, W. J., and Bayley, F. J., 1988, “Turbulence Measurements in Turbine Blade Passages and Implications for Heat Transfer,” *ASME J of Turbomachinery*, vol. 110, pp. 73-79.

Radomsky, R. W. and Thole, K. A., 1998, “Effects Of High Freestream Turbulence Levels and Length Scales on Stator Vane Heat Transfer,” ASME Paper No. 98-GT-236.